Temporal Order in Periodically Driven Spins in Star-Shaped Clusters

Soham Pal, Naveen Nishad, T. S. Mahesh, and G. J. Sreejith

Indian Institute of Science Education and Research, Pune 411008, India

We experimentally study the response of star-shaped clusters of initially unentangled $N = 4$, 10, and 37 nuclear spin-1/2 moments to an inexact π-pulse sequence and show that an Ising coupling between the center and the satellite spins results in robust period-2 magnetization oscillations. The period is stable against bath effects, but the amplitude decays with a timescale that depends on the inexactness of the pulse. Simulations reveal a semiclassical picture in which the rigidity of the period is due to a randomizing effect of the Larmor precession under the magnetization of surrounding spins. The timescales with stable periodicity increase with net initial magnetization, even in the presence of perturbations, indicating a robust temporal ordered phase for large systems with finite magnetization per spin.

Spontaneous symmetry-breaking is a central notion in many body physics, allowing us to explain several natural phenomena, such as formation of a magnet or ice crystals. While there are many systems in which the underlying spatial symmetries are broken, resulting in various crystalline phases, and a few classical systems that exhibit spontaneous temporal oscillations, it was only recently that the possibility of spontaneous breaking of time translation symmetry in quantum systems was considered. The initial proposals [1] for realizing a spontaneous breaking of continuous time translation symmetry were later shown to be forbidden in static equilibrium systems [2,3]. However, in the attempt to understand quantum thermodynamics of driven systems, it was realized that an externally driven, disordered, interacting spin system can stabilize a phase that spontaneously breaks the discrete time translation ($\mathbb{Z}$) symmetry of the system to a subgroup $n\mathbb{Z}$ [4–7]. The phenomenon was soon experimentally realized in trapped cold-atom systems that mimic a long-range interacting disordered spin-half chain [8] and in dense collections of randomly interacting nitrogen vacancy centers embedded in diamond [9,10]. While this Letter was under review, similar observations were also realized in other solid NMR experiments [11].

In this Letter, we report on the observation of robust period-2 oscillations of magnetization in a cluster of nuclear spins in a simple star-shaped geometry, with a central spin interacting with N surrounding satellite spins via Ising interactions mediated by the electron cloud in the molecule. The satellite spins do not interact with each other. Spins in each molecule show magnetization oscillations of period 2, as expected, when subjected to a sequence of transverse π pulses (pulses that rotate every up or down spin by π rad). However, the Ising interactions within the cluster result in the period rigidly locking onto two, even under a sequence of inexact π pulses (pulses that rotate by an

amount $\pi - e$). Simulations of an isolated cluster show that the period is robust even in the presence of small perturbations and disorder that break the symmetries of the model. For the present Letter, we perform nuclear magnetic resonance (NMR) experiments on acetonitrile, trimethyl phosphite (TMP), and tetrakis(trimethylsilyl) silane (TTSS) containing 4,10, and 37 spins [Figs. 1(a)–1(c)] [12]. The experiments are performed on ensembles of $\sim 10^{15}$ molecules with a distribution of initial states, described by a direct product density matrix. High precision ensemble average magnetization measurements of central or satellite spins can be performed using free-induction decay signals. Period-2 oscillation of individual spins results in corresponding oscillations of the ensemble average magnetization. Control experiments performed on molecules that contain a spinless isotope at the center show oscillations with frequencies that linearly vary with the deviation e, showing that the robustness of the period originates from interaction with the central spin. In the following, unless units are made explicit, frequencies are in units where the time period $T = 1$.

Model and numerical results.—The unitary operator evolving the state of the cluster between successive steps is given by

$$U(J, \theta; t) = \exp\left(-\frac{\iota J t}{\hbar} S_0^z \sum_{i=1}^{N-1} S_i^z\right) \quad \text{for } t \in [0, T),$$

$$U(J, \theta; T) = \exp\left(-\iota\theta \sum_{i=0}^{N-1} S_i^x\right) \exp\left(-\frac{\iota J T}{\hbar} S_0^z \sum_{i=1}^{N-1} S_i^z\right),$$

$$(1)$$

where J, T, and θ are the Ising interaction strength, time period, and the rotation angle characterizing the pulse. S_i^μ are spin operators. Site index $i = 0$ labels the central spin
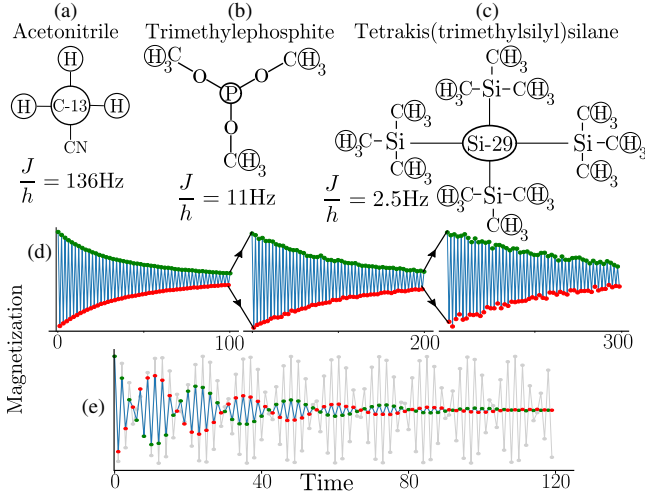
FIG. 1. Molecules used in the experiments: (a) acetonitrile, (b) trimethyl phosphite, and (c) tetrakis(trimethylsilyl)silane, with the 4, 10, and 37 NMR active nuclei encircled. (d) Experimentally measured magnetization $\langle S_i^z \rangle$ of satellite spins of TMP for the pulse sequence in Eq. (1) with $JT/\hbar = 6.5$ and $\theta = \pi - 0.1$. Red (green) dots show the magnetization at odd (even) time steps. For visibility in the plot, the y axis has been rescaled at every 100th time step. (e) Blue line shows experimentally measured magnetization oscillations of free or noninteracting spins of protons in acetonitrile that contain a spinless C-12 central spin, at a pulse angle $\theta = \pi - 0.27$. Gray lines indicate the expected response in the absence of a bath.

(see [13] and Supplemental Material [14] for a description of liquid-state NMR, which realizes the unitary).

We will label the deviation from π pulse by $e = \pi - \theta$. To simplify the discussion below, it is useful to temporarily switch to a toggling frame of reference in which the basis of every spin rotates by an angle π about the x axis after each pulse. Because of the $\mathbb{Z}_2$ symmetry of the model, the unitary operator in the rotating basis retains the same form as in Eq. (1), but with a reduced pulse angle $e = \pi - \theta$; i.e., the spins in the rotating basis see a unitary operator $U(J, -e; t)$. A constant z magnetization of all spins in the rotating basis picture corresponds to a period-2 oscillation of all physical spins. Numerical simulations indeed show that a finite magnetization is maintained under a sequence of weak pulses (pulse angle $-e$). Presented below is a semiclassical picture inferred from numerical simulations (Fig. 2).

For simplicity, we will consider the time evolution starting from a fully polarized initial state under a sequence of small pulses $\theta = -e$ (corresponding to $\theta = \pi - e$ experienced by the physical spins). During $0 < t < T$, the spins do not evolve, as the state is an eigenstate of the unitary evolution [Eq. (1)]. At time $t = T$, the pulse rotates every spin by an angle e away from the z axis, as shown on the Bloch sphere (see Fig. 2). During $T < t < 2T$, the central spin, which is tilted away from the z axis, evolves under the Hamiltonian $H \approx -J\langle M_s \rangle S_0^z$,
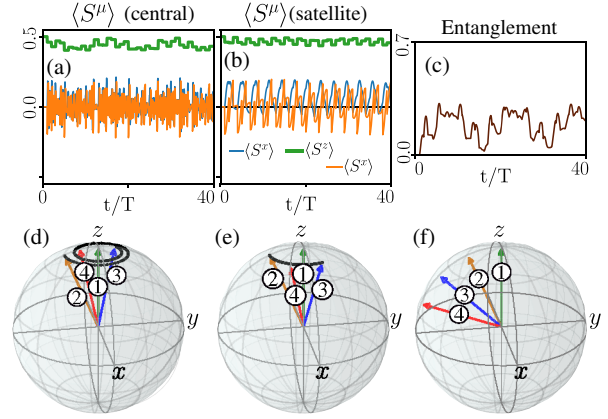

FIG. 2. Numerical simulations of spins in the rotating basis. (a),(b) Time dependence of the expectation values of the three spin components of a satellite (b) and central (a) spin for a system with $N = 8$ spins, $[(JT)/\hbar] = 4$, and pulse angle $\theta = e = 0.4$. Initial state is the fully z polarized state. (c) Entanglement entropy of the central spin. (d) Bloch sphere representing the spin components of a central spin (of a six spin cluster) at times $t = 0$, T^+, $2T^-$, and $2T^+$; $+ (-)$ labels the time just after (before) the pulse. Sequence of intermediate dots track the evolution between time $t = T$ and $2T$. (e) Same as (d) but for a satellite spin. (f) Bloch vectors for a single isolated spin at successive time steps.

where M_s is the net z magnetization of the satellite spins, resulting in a Larmor-like precession as shown in Fig. 2(d). The orientation of the central spin at $t = 2T^-$ depends on the amount of precession $[(JT\langle M_s \rangle)/\hbar]$. The e pulse at $t = 2T$ now brings the spin vector to a polar angle $0 < \theta < 2e$. Owing to the precession, the successive e pulses can now cancel each other. In contrast, in a set of noninteracting spins, the angles always add constructively leading to a steady increase in the polar angle [ne after n pulses; see Fig. 2(f)]. Thus, the randomizing effect of the interaction-induced Larmor precession, causes the polarization of the central spin to survive longer than that of an isolated spin. We expect the same effect to be seen also on the surrounding spins, except that they precess under the magnetization of the central spin alone, resulting in a slower precession of the satellite spins compared to the central spin [Fig. 2(f)]. The constant sign of the Bloch-vector component $\langle S^z \rangle$ in the rotating basis implies a period-2 oscillation of the physical spin orientation [Figs. 2(a) and 2(b)].

Such a semiclassical picture assumes that the central spin is not maximally entangled with the surrounding spins, as otherwise the Bloch vector may vanish in length even when the polar angle is conserved. As shown in Fig. 2(c), the von Neumann entropy of the central spin stays below maximum, ensuring finite Bloch vectors. Simulations of the small systems at much longer timescales using exact diagonalization indicate that entanglement of the system does not rise for timescales that increase exponentially with system size [Figs. 3(c) and 3(d)].
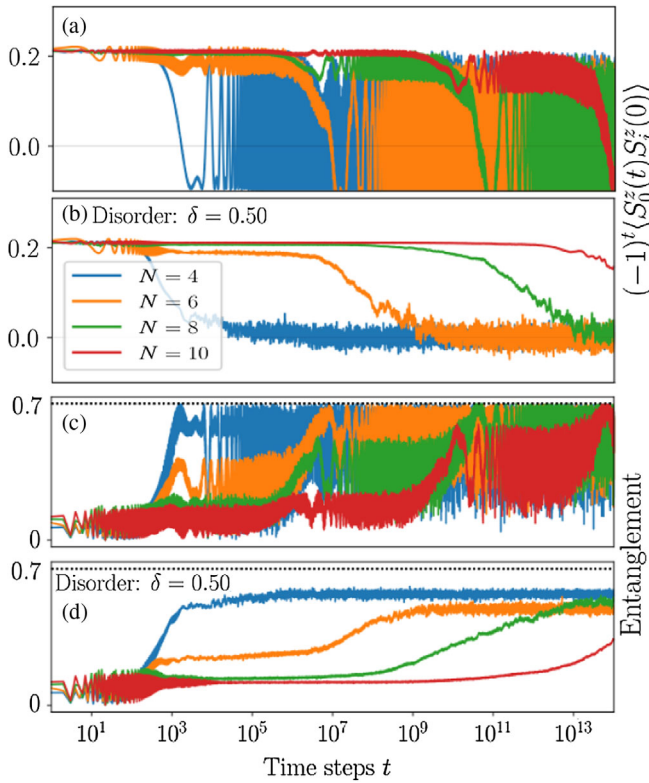
FIG. 3. (a),(b) Time dependence of cross correlation [multiplied by $(-1)^t$] between the central spin S_0^z and a satellite spin S_i^z from simulations of systems of different sizes [$JT/\hbar = 4$, $e = 0.05$, $\psi = R_x(\pi/8)|\uparrow\uparrow\ldots\rangle$, $R_x(\pi/8)$ being the rotation of all spins by $\pi/8$ about x]. Disorder strengths are 0 (a),(c) and 0.5 (b),(d). (c),(d) Entanglement entropy of the central spin. Disorder averaging has been performed in (b),(d).

In the following, we will use the physical spin basis. To explore the stability of the period to perturbations other than e, we numerically simulated a pure spin system with a time-independent perturbation to the Hamiltonian of the form $\sum_i h_i^x S_i^x + h_i^z S_i^z$. The quenched disorder h_i^x and h_i^z were picked uniformly from $[-\delta/2, \delta/2]$ and $[0, \delta]$ (in units where $T/\hbar = 1$). To compare the response of different system sizes, we fix the average magnetization per spin. We found that, in all cases, the timescale in which there was a dominant period-2 oscillation appeared to grow exponentially with system size [Fig. 3(b)]. Similar increases in timescales were also observed in simulations with disorder-free perturbations of the form $h_z \sum S_i^z$ and $J_x \sum S_i^x S_{i+1}^x$ [14]. The timescales with a stable period are higher when the initial state of the spin cluster had a larger total magnetization. Slow heating and stability in this disorder-free system is likely to be associated with a prethermal regime similar to that in Refs. [15,16]. However, unlike the high frequency case discussed there, the experiments here are performed at low frequencies ($JT > 1$). Cross correlation between the central and satellite spins [Figs. 3(a) and 3(b)] shows that different

spins oscillate in synchrony, suggesting that the robustness of the period is a collective behavior of all spins.

For small e and the $\mathbb{Z}_2$ symmetric unitary [Eq. (1)], origin of the period-2 oscillations at finite deviation e can be understood in a manner similar to that described in Ref. [5]. The Floquet unitary describing the periodic drive commutes with the parity operator $P = \prod 2S_i^x$ and therefore the quasienergy eigenstates have a parity quantum number ± 1. The quasienergy states of the system at $\theta = 0$ occur in degenerate quasienergy pairs of opposite parity $\psi_\pm = |\sigma_0, m\rangle \pm |-\sigma_0, -m\rangle$, where $|\sigma_0, m\rangle$ is a state with central and satellite spins in an eigenstate of S_0^z and $\sum_{i=1}^{N-1} S_i^z$ with eigenvalues σ_0 and m. At small finite pulse angle $\theta = e$, the quasienergy degeneracy is broken in a manner that depends on the magnetization $|m|$ as $\sim e^{2|m|+1}$. In the presence of a sequence of inexact π pulses $\theta = \pi - e$, the unitary is $U(J, \pi - e; T) = PU(J, -e; T)$, for which the states $\psi_\pm$ have quasienergies separated by $\pi + \mathcal{O}(e^{2|m|+1})$. A polarized direct product initial state $|\sigma_0, m\rangle$ is a symmetric or antisymmetric linear combination of the states $\psi_\pm$. As a result, the unitary for inexact π pulses acts on such a polarized state to flip the orientation of all the spins at each time step

$$U|\sigma_0, m\rangle = U(\psi_+ \pm \psi_-) \sim \psi_+ \pm e^{-\iota\pi}\psi_- = |-\sigma_0, -m\rangle,$$
(2)

resulting in a period-2 magnetization oscillation. Better degeneracies of the higher magnetization initial states explain why initial states with larger magnetization show stable periodicity for longer timescales. Subleading oscillations of other frequencies originate from mixing of $\psi_\pm$ with states of smaller magnetizations.

NMR setup.—The spin systems used for the experiments—acetonitrile, TMP, and TTSS—are prepared in the solvents dimethyl sulfoxide or deuterated chloroform. The experiments are carried out at 300 K in a Bruker 400 MHz NMR spectrometer equipped with an UltraShield superconducting magnet of strength 9.39 T. The unitary of Eq. (1) is realized in a doubly rotating frame [13,14]. The θ pulses are realized by simultaneous resonant, short duration radio frequency pulses on all spins. The pulse duration can be tuned to control θ. Interaction parameter $JT/\hbar$ can be set by tuning the time period T. After n pulses, any residual transverse magnetization is destroyed using a pulsed field gradient, and the final magnetization $\langle S^z \rangle$ is rotated into the transverse direction with the help of a $\pi/2$ detection pulse. The NMR signal is then detected as the oscillatory emf induced in a probe coil due to the precessing transverse magnetization about the Zeeman field [14,17]. During each period, the measurement was performed immediately after the pulse.

Initial states in the experimental ensemble of $\sim 10^{15}$ molecules can be described by mixed state of the form $\rho = \prod_{i=0}^{N-1} \otimes \rho_i$, where $\rho_i = \frac{1}{2}(\mathbb{1} + \epsilon\sigma_i^z)$, and the purity

$\epsilon \approx 10^{-5}$, σ^z being the Pauli matrix. The purity is inferred from the thermal equilibrium distribution at the magnetic field strength inside the spectrometer. Note that, while the ensemble average magnetization is small, the ensemble contains subensembles of all possible initial magnetizations $-N/2 \leq M \leq N/2$, with a marginally higher fraction (parameterized by ϵ) with a positive sign. Clusters with finite magnetization $|M|$ show stable period-2 oscillations, which collectively reflect in the ensemble average measurements.

Results and discussion.—Figure 4 shows the measured satellite spin magnetizations in TMP and acetonitrile for an interaction parameter $(JT)/\hbar = 20.7$ ($J/h = 11$ Hz, $T = 0.3$ s). Magnetization oscillations on TMP [Figs. 4(a)–4(c)] show a clear peak at frequency half (subharmonic peak), whose height decreases with increase in the deviation e, vanishing at $e \approx 0.4\pi$ in agreement with the simulations. There are no discernible peaks in the spectrum at frequencies $[(\pi \pm e)/2\pi]$ expected from noninteracting spins. Fourier transforms were taken using standard FFT algorithms applied to the data from the chosen time window. For comparability, magnetization data were normalized such that initial magnetization was one.

The rf pulses have $\pm 5\%$ distribution of θ values around the nominal value, due to the spatial inhomogeneity of the rf field over the volume of the sample. The experimental system suffers from decoherence due to coupling to an external thermal bath. This could explain the decay of the oscillation amplitudes with time [18]. Apart from this decay, the magnitude of the subharmonic peaks in each time window match the simulations. Interestingly, the decay time decreases steadily with e [Fig. 4(c)].

The acetonitrile sample contains a mixture with 99% of the molecules carrying a spinless C-12 and 1% of the molecules containing a spinful C-13 atom in the methyl group. Although the NMR signal has contributions from the satellite spins of both isomers, their contributions can be separated in the frequency domain of the induced emf oscillations during the final measurement process, thanks to the presence or absence of interaction with the central spin, and thus they can be analyzed separately. Experiments on acetonitrile were performed at the parameter $(JT)/\hbar \approx 17.1$ ($J/h = 136$ Hz, $T = 0.02$ s). Figure 4(e) shows the Fourier transforms of magnetization of the satellite spins in acetonitrile that contain a spinfull C-13 central atom. Figure 4(f) shows the Fourier transform of the magnetization of the satellite spins in molecules containing a spinless C-12 central atom. In the absence of a central spin with which the satellites can interact, they oscillate like isolated spins with a frequency that varies linearly with e. The absence of a stable period in this noninteracting system clearly shows that the stability of the period observed in other clusters arises from interactions. Figure 5 shows the results for magnetization measurements of the central Si-29 spin of the TTSS molecule, which has $N = 36$ satellite spins around the central atom. Experiments were performed at $JT/\hbar \approx 4$ ($J/h = 2.5$ Hz, $T = 0.25$ s).

We have experimentally demonstrated that stable temporal order can be realized in NMR spin clusters. Absence
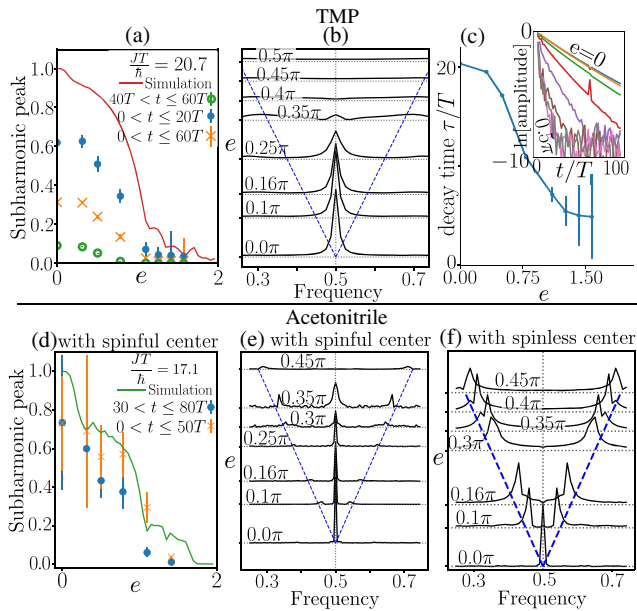

FIG. 4. Experimentally measured satellite spin magnetization $\sum_{i=1}^{N-1} \langle S_i^z \rangle$. (a),(d) Magnitude of the subharmonic peak upon varying e in TMP and acetonitrile. Solid continuous lines show results from simulations. Different markers indicate Fourier transforms of experimental measurements in different time windows. (b) Waterfall plot of the Fourier spectrum (time window $0 < t < 80T$) of the experimentally observed magnetization of TMP at different deviations e. Dashed blue lines indicate the location of peaks expected for a free spin. (c) Variation of the decay time of the experimentally observed magnetization amplitude with e for TMP. (e),(f) Same as (b) but for acetonitrile with a spinful C-13 (e) and spinless C-12 (f) atom at the center.
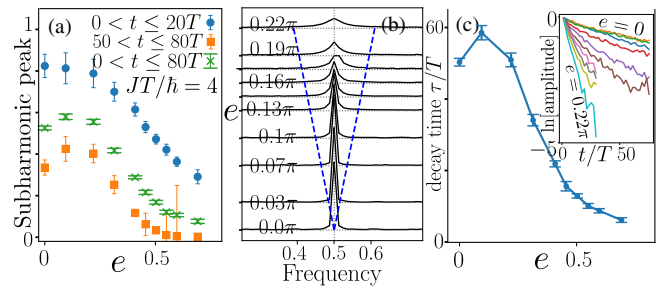

FIG. 5. Experimental values of central spin magnetization $\langle S_0^z \rangle$ in TTSS. (a) Subharmonic peak strength as a function of the deviation e. Different markers indicate Fourier transforms in different time windows. (b) Waterfall plot of the Fourier spectrum of the experimentally observed central spin magnetization at different e. Blue dashed line shows the location of the Fourier peaks expected for free spins. (c) Decay timescale as a function of e. (Inset) A semilog plot of the amplitude of magnetization as a function of time.

of a stable period in the control experiment in C-12 acetonitrile shows that stability of the period requires interactions between the spins (as in C-13 acetonitrile). Though bath effects and other perturbations in the experiment lead to a magnetization decay with time, interestingly, the period appears to be unaffected. Stability of the period in the spin cluster improves with increase in total initial magnetization. Therefore, large systems with finite initial magnetization per spin should show a stable temporal ordered phase. The stability of the oscillations in such systems can be interpreted as an error correction on the pulse sequence and may find potential applications towards robust quantum information processing [19].

[1] F. Wilczek, Quantum Time Crystals, Phys. Rev. Lett. **109**, 160401 (2012).

[2] P. Bruno, Comment on "Quantum Time Crystals," Phys. Rev. Lett. **110**, 118901 (2013).

[3] H. Watanabe and M. Oshikawa, Absence of Quantum Time Crystals, Phys. Rev. Lett. **114**, 251603 (2015).

[4] V. Khemani, A. Lazarides, R. Moessner, and S. L. Sondhi, Phase Structure of Driven Quantum Systems, Phys. Rev. Lett. **116**, 250401 (2016).

[5] D. V. Else, B. Bauer, and C. Nayak, Floquet Time Crystals, Phys. Rev. Lett. **117**, 090402 (2016).

[6] C. W. von Keyserlingk, V. Khemani, and S. L. Sondhi, Absolute stability and spatiotemporal long-range order in Floquet systems, Phys. Rev. B **94**, 085112 (2016).

[7] N. Y. Yao, A. C. Potter, I.-D. Potirniche, and A. Vishwanath, Discrete Time Crystals: Rigidity, Criticality, and Realizations, Phys. Rev. Lett. **118**, 030401 (2017).

[8] J. Zhang, P. W. Hess, A. Kyprianidis, P. Becker, A. Lee, J. Smith, G. Pagano, I.-D. Potirniche, A. C. Potter, A. Vishwanath, N. Y. Yao, and C. Monroe, Observation of a discrete time crystal, Nature (London) **543**, 217 (2017).

[9] S. Choi, J. Choi, R. Landig, G. Kucsko, H. Zhou, J. Isoya, F. Jelezko, S. Onoda, H. Sumiya, V. Khemani, C. von Keyserlingk, N. Y. Yao, E. Demler, and M. D. Lukin, Observation of discrete time-crystalline order in a disordered dipolar many-body system, Nature (London) **543**, 221 (2017).

[10] W. W. Ho, S. Choi, M. D. Lukin, and D. A. Abanin, Critical Time Crystals in Dipolar Systems, Phys. Rev. Lett. **119**, 010602 (2017).

[11] J. Rovny, R. L. Blum, and S. E. Barrett, following Letter, Observation of Discrete-Time-Crystalline Signatures in an Ordered Dipolar Many-Body System, Phys. Rev. Lett. **120** 180603 (2018); ^{31}P NMR study of discrete time-crystalline signatures in an ordered crystal of ammonium dihydrogen phosphate, Phys. Rev. B **97**, 184301 (2018).

[12] V. R. Pande, G. Bhole, D. Khurana, and T. S. Mahesh, Strong algorithmic cooling in large star-topology quantum registers, Phys. Rev. A **96**, 012330 (2017).

[13] M. H. Levitt, *Spin Dynamics: Basics of Nuclear Magnetic Resonance* (John Wiley & Sons, New York, 2001).

[14] See Supplemental Material at http://link.aps.org/supplemental/10.1103/PhysRevLett.120.180602 for a summary of the liquid NMR physics as well as additional numerical results.

[15] D. V. Else, B. Bauer, and C. Nayak, Prethermal Phases of Matter Protected by Time-Translation Symmetry, Phys. Rev. X **7**, 011026 (2017).

[16] D. A. Abanin, W. De Roeck, and F. Huveneers, Exponentially Slow Heating in Periodically Driven Many-Body Systems, Phys. Rev. Lett. **115**, 256803 (2015).

[17] J. Cavanagh, *Protein NMR Spectroscopy: Principles and Practice* (Academic, New York, 1996).

[18] A. Lazarides and R. Moessner, Fate of a discrete time crystal in an open system, Phys. Rev. B **95**, 195135 (2017).

[19] S. Choi, N. Y. Yao, and M. D. Lukin, Quantum metrology based on strongly correlated matter, arXiv:1801.00042.